Green Synthesis of Nanoscale Zero-Valent Iron Aggregates for Catalytic Degradation of Textile Dyes

Sanja Panić[1] · Mirjana Petronijević[1] · Jelena Vukmirović[1] · Nenad Grba[2] · Saša Savić[3]

Abstract

The application of zero-valent iron nanoparticles (nZVI) is an area of growing interest, especially in the remediation processes of waters of different origin. The standard synthetic procedure for nZVI involves the chemical reduction of Fe^{2+} or Fe^{3+} with the solution of a strong reducing agent. This type of synthetic route leads to the formation of new toxic species. The green synthesis of nZVI using plant extracts is, therefore, an excellent alternative to the above-mentioned conventional methods. Within the scope of this work, the amorphous nZVI was synthesized by green tea mediated single-step method from Fe^{3+} as precursors, denoting an eco-friendly approach. Additionally, the physico–chemical characterization (TEM, SEM/EDS, size of particles/aggregates, XRD, BET) of nZVI was performed. The catalytic activity of the obtained nZVI was tested in a Fenton-like reaction of the removal/degradation of three representative industrial textile dyes (methylene blue, methyl orange and bromothymol blue) from water. In order to optimize the process parameters, the effect of homogenization treatment, nZVI and H_2O_2 concentration on catalytic performance were also done followed by degradation kinetic study using four different models. The results of this work have shown the exceptionally high efficiency of the green nZVI which is reflected in almost complete degradation of all tested dyes within very short period of time, despite their amorphous nature, aggregates arrangement and very low specific surface area. Furthermore, the examined degradation kinetics has excellently followed the BMG model, indicating that the degradation process of the investigated dyes proceeds via two stages (two-stage pattern)—a fast one and a much slower one, regardless of the used reaction conditions. Based on all gained results, particular degradation mechanisms were proposed.

Graphical Abstract
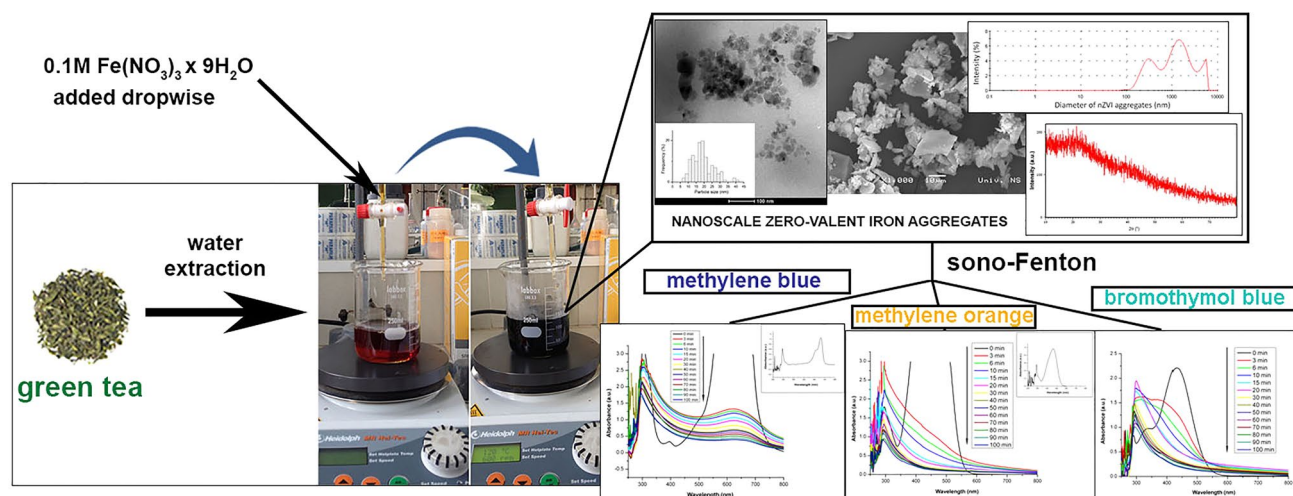
Extended author information available on the last page of the article

1 Introduction

The application of nanotechnology in environmental remediation processes is becoming increasingly important, primarily due to the reduction of production costs, as well as the increasing efficiency compared to the traditional methods used so far. Today, the term nanoremediation refers to the use of highly reactive, mostly catalytic nanomaterials in order to remove various pollutants from the air, water or soil. In this sense, the use of zero-valent iron nanoparticles (nZVI) is a field of growing interest, especially in the field of the remediation of waters of different origin [1–5]. Prior to the synthesis of zero-valent iron at the nanoscale, the microscale zero-valent iron (micro-ZVI) was widely used in many environmental processes, primarily in its pristine (unmodified) form. However, due to some limitations which appeared during its engineering applications, various methods have been proposed in order to overcome these drawbacks and promote the reactivity of macro-ZVI, especially in water remediation processes. These methods included acid washing, chemical strengthening (including sulfidation), physical fields strengthening, etc. For example, Liang et al. [6] have studied the reactivity of sulfide modified micro-ZVI with and without the magnetic field in the process of selenite removal from water samples. According to their results, coupled sulfidation of ZVI and magnetic field represents an excellent method to enhance the reactivity of micro-ZVI in order to be also successfully used in other remediation processes. Among the previously mentioned methods developed for the promotion of the reactivity of ZVI, the synthesis of its nanoscale form (nZVI) can be considered as a very popular method due to various beneficial properties of these particles that coincide with the persistent requirements for the development of innovative remediation techniques. The first method for the synthesis of nZVI was published in 1997 [7]. Later research has shown that these particles have a large ratio of specific surface area and mass, and therefore greater reactivity compared to particles from the domain of microsizes. In addition, the size of nanoparticles is smaller than most pores of porous media, so they can be more easily transported to the contamination zone [8]. They are also characterized by low cost, non-toxicity, simple production and high efficiency of the removal/degradation of a wide range of chemical pollutants, including azo dyes, pigments [4, 5, 9], nitroamines, nitrates, perchlorates, heavy metals [10, 11], metalloids, etc. [12]. The most commonly used method for obtaining nZVI is the reduction of Fe^{2+} or Fe^{3+} with the solution of a strong reducing agent, such as sodium borohydride. However, during chemical synthesis, new toxic species are formed, which are very difficult to separate from the formed Fe nanoparticles and

can cause additional pollution [13]. In addition, flammable gas (hydrogen) can be formed during the process, which is another disadvantage of this method [14]. Expensive reagents also limit its industrial application. Due to the mentioned shortcomings, the method of green synthesis represents a good alternative. It is an environmentally friendly and economically acceptable process in which the reduction of iron ions is performed using the extracts of natural products (leaves, bark or other parts of plants) that are rich in polyphenols and have a high reducing power to convert Fe^{2+} and Fe^{3+} into nZVI [4, 14–17]. When performing this method, high pressures are not required, as well as additional energy—the synthesis can be performed at room temperature [13]. Compared to traditional synthesis procedures, the green synthesis of nZVI is faster, simpler, cheaper and non-toxic. The polyphenolic matrix protects the particles from oxidation and excessive agglomeration, and the resulting products are not harmful to human health and the environment [18, 19]. Plant residues that are considered waste can also be used as a source of polyphenols.

In the last few years, nanoremediation procedures have been intensively investigated using Advanced Oxidation Processes (AOP). These processes are based on the ″in situ″ formation of hydroxyl radicals that exhibit strong oxidative capacity to complex organic molecules. The most commonly used AOP is the Fenton process in which Fe^{2+} is used as a catalyst and H_2O_2 as an oxidant [20, 21]. The advantages of this process are the simplicity of performance, non-toxicity, as well as the possibility of performance at room temperature and atmospheric pressure. However, the limiting factors of application are high cost, limited optimal pH range, the presence of inorganic anions (SO_4^{2-}, Cl^-) in water after treatment, a high concentration of Fe^{2+} (50–80 ppm), as well as the slow regeneration of these ions. Also, the precipitation of Fe^{3+} to $Fe(OH)_3$ produces a large amount of sludge, which reduces the efficiency of the process and causes secondary pollution [22]. In order to overcome the mentioned shortcomings, the Fenton process was improved by the use of other homogeneous or heterogeneous catalysts (except Fe^{2+})—Fe^{3+}, Cu^{2+}/Cu, pyrite, as well as zero-valent Fe. All these processes belong to the so-called Fenton-like processes. The efficiency of Fenton and Fenton-like processes can be increased by applying different physical fields/phenomena, and accordingly several types of Fenton processes can be distinguished—the photo-Fenton, electro-Fenton, cavitation (ultrasonic)-Fenton and microwave-Fenton process [20–22]. The application of nZVI in heterogeneous Fenton-like processes is becoming more intensive due to several advantages over the homogeneous Fenton reaction. First of all, the use of Fe nanoparticles instead of the corresponding salts avoids the introduction of inorganic anions into the water. Also, nZVI has the role of a

slow-release source of Fe^{2+}, and further the formed Fe^{3+} reacts again with nZVI and enables the regeneration of Fe^{2+}. In this way, the problem of the deficiency of these ions in the system is solved, and the concentration of both types of iron ions in wastewater is reduced in relation to the homogeneous process. Since there is no need for additional wastewater treatment, the heterogeneous process is characterized by a lower cost.

One of the most important applications of nZVI as a catalyst in nanoremediation processes involves the removal of organic dyes from polluted water and wastewater using a process similar to Fenton. Organic dyes are a very widespread group of water pollutants and most of the wastewaters containing dyes come from the textile industry [23]. In the natural environment, these dyes are very stable and their biological degradation is difficult [24]. Each dye has its own chemical structure. The group of atoms or electrons that is responsible for the color in a molecule is called a chromophore, and the compounds that contain this group are called chromogens. The mechanism of degradation of textile dyes in a process similar to Fenton is based on the exchange of electrons between nZVI (electron donor) and dye molecules (electron acceptor). nZVI is oxidized to Fe^{2+} and Fe^{3+} in aqueous solution, and the resulting hydroxyl and hydrogen ions then react with dye molecules, breaking the bond in the chromophore and decolorizing the treated solution [24]. The efficiency of dye degradation depends on the pH value, the amount of nZVI, the initial dye concentration, the H_2O_2 concentration and the temperature. Recently, a process similar to Fenton is increasingly being combined with ultrasound, and this method is a good alternative for increasing the efficiency of the degradation process.

Within this study, three widely used dyes in textile industry were subjected to H_2O_2 oxidation/degradation in the presence of green zero-valent iron nanocatalyst under different reaction parameters. Methylene blue was selected as a model for cationic dyes, while methyl orange is a typical representative of anionic dyes. Bromothymol blue, often employed as a pH indicator is a useful probe compound since it can only be chemically degraded via free radical pathways. The main objective of this work was to examine the applicability of green synthesized nZVI as a Fenton-like catalyst in order to contribute to the development of rapid, simple and sustainable remediation techniques. To the best of our knowledge, this is the first paper demonstrating the excellent performance of the used green heterogeneous nanocatalyst in all tested processes, emphasizing that some characteristics of nZVI usually stated in the literature as the main drawbacks of this type of catalyst (tendency to form aggregates, very low specific surface area, amorphous nature) do not have to be a prerequisite for a reduced catalyst performance.

2 Experimental

2.1 Materials and Chemicals

All the chemicals used in this study were analytical reagent grade or higher, purchased from Sigma-Aldrich and applied without any further pretreatment: $Fe(NO_3)_3 \times 9H_2O$, ACS reagent, $\geq 98.0\%$; Hydrogen peroxide 30% stabilized; Salicylic acid, ACS reagent, $\geq 99.0\%$; Methylene blue (1.59270); Methyl orange (1.01322) and Bromothymol blue (1.03026). Green tea was purchased from the local supermarket.

2.2 The Green Synthesis of Zero-Valent Iron Nanoparticles (nZVI)

The synthesis of zero-valent iron nanoparticles (nZVI) was performed according to the methodology published by [25] with some modifications. A 0.1 M solution of $Fe(NO_3)_3 \times 9H_2O$ was used as a precursor of iron. The green tea extract (the concentration of 0.02 g/ml) was prepared by boiling the commercial green tea in a certain volume of water. The cooled tea was then filtered through a Buchner funnel. The green synthesis of nZVI was performed at room temperature by stepwise dripping of iron precursor into the green tea extract in a volume ratio of 1: 4, respectively. During the synthesis, the reaction mixture was kept under constant magnetic stirring (600 rpm). After adding the first drop of iron precursor, the color of the green tea extract changed from yellow-orange to black, which is an indication of the formation of nZVI.

For TEM, SEM, XRD and textural characterization, the synthesized nZVI sample was dried in an oven at 80 °C for 24 h, while the particle size distribution on the Zetasizer was determined immediately after the synthesis, in the liquid phase.

2.3 The Physico-Chemical Characterization of nZVI

The structure and morphology of the nZVI sample were examined by transmission electron microscopy (FEI TEC-NAI G2 20X-TWIN Transmission Electron Microscope) (TEM) and scanning electron microscopy (SEM) (JEOL JSM-6460LV at 25 kV), while the elementary analysis was performed by the method of microanalysis using Energy-Dispersive X-ray Spectroscopy (EDS) (in combination with the SEM method). Textural characteristics were determined by means of low temperature N_2 adsorption/desorption (LTNA) method, using He as a carrier gas (Micromeritics ASAP 2010). The crystal structure of the nZVI sample was examined by X-ray diffraction analysis (XRD) on a Rigaku Miniflex 600 diffractometer using CuKα radiation of a

wavelength of λ = 0.15406 nm. The analysis was performed in the interval of 10–80° 2θ, with a step of 0.3° and with a retention time of 3 s. The particle size distribution of the nZVI sample was determined using the Malvern ZetaSizer Nano 2009, which has the ability to measure particle sizes in the range of 0.4 nm to 6 μm based on the principle of dynamic light scattering (DLS).

2.4 The Determination of the Concentration of Synthesized nZVI in the Green Tea Extract

In order to determine the concentration of synthesized nZVI in the green tea extract, the resulting mixture was centrifuged at 10,000 rpm, and the supernatant was then used to determine the concentration of residual (unreduced) Fe^{3+}. The method for determining the concentration of Fe^{3+} is based on the reaction of forming a purple complex between Fe^{3+} and salicylic acid. The resulting complex has maximum absorption in the visible region of the spectrum at a wavelength of 526.5 nm. The concentration of residual Fe^{3+} was measured on a UV–VIS spectrophotometer (CECIL 2021) based on the previously obtained calibration curve.

2.5 The Degradation of Textile Dyes in the Presence of nZVI in a Heterogeneous Fenton-Like Process

Previously synthesized nZVI sample was used in the process of degradation of three textile dyes—methylene blue (MB), methyl orange (MO) and bromothymol blue (BTB). The degradation reaction was performed in an Erlenmeyer flask at room temperature by mixing 100 ml of a 100 ppm dye solution with nZVI and hydrogen peroxide solution. In order to determine the influence of the homogenization method on the Fenton-like process, the reaction was performed on a magnetic stirrer and in an ultrasonic bath, under the following experimental conditions: 100 ml methylene blue solution (100 ppm), nZVI concentration in dye solution 2 ppm, and H_2O_2 concentration in dye solution 600 ppm. It has to be emphasized here that the influence of magnetic field on the course of the reaction due to the utilization of magnetic stirrer has not been taken into consideration. The optimization of the concentration of nZVI and H_2O_2 in the sono-degradation process of methylene blue was performed by varying the mentioned concentrations in the range of 0–20 ppm for nZVI and from 0 to 600 ppm for H_2O_2. With the previously selected reaction parameters, the process was also performed for methyl orange and bromothymol blue. The change in the concentration of each individual dye was monitored during the process by sampling at defined time intervals and measuring on a UV–VIS spectrophotometer (CECIL 2021), based on previously obtained calibration curves—at 664 nm for methylene blue, 465 nm for methyl orange and 432.5 nm for bromothymol blue. Also, the pH value of the dye solution was measured at the same time, as well as the reaction mixture at the beginning and end of the Fenton-like process.

UHPLC-DAD-ESI-MS/MS analysis was performed using a Thermo Scientific liquid chromatography system (Mass Spectrometry Laboratory, University of Nis, Leskovac, Serbia) composed of a quaternary pump with a degasser, a thermostated column compartment, an autosampler, and a diode array detector connected to LCQ Fleet Ion Trap Mass Spectrometer (Thermo Fisher Scientific, San Jose, California, USA) equipped with electrospray ionization (ESI). Xcalibur (version 2.2 SP1.48) and LCQ Fleet (version 2.7.0.1103 SP1) software were used for instrument control, data acquisition, and data analysis. Separations were performed on a Hypersil gold C18 column (50×2.1 mm, 1.9 μm) obtained from Thermo Fisher Scientific.

The mobile phase consisted of (A) water (Fisher Chemical, HPLC grade) + 0.1% formic acid (Carlo Erba, Italy) and (B) acetonitrile (Fisher Chemical, LC–MS grade). A linear gradient program at flow rate of 0.25 ml/min was used 0–2 min from 10 to 20% (B), 2–4.5 min from 20 to 90% (B), 4.5–4.8 min 95% (B), 4.8–4.9 min from 90 to 10% (B) and 4.9–12 min 10% (B).

The injection volume and temperature of the column were 5 μl and 25 °C, respectively. The mass spectrometer was operated in positive and negative ion mode as the method of identification. MS spectra were acquired by full range acquisition in the 50–1000 m/z range. For the fragmentation study, a data-dependent scan was performed by deploying the collision-induced dissociation (CID). The normalized collision energy of the collision-induced dissociation (CID) cell was set at 25 eV. Compounds were identified according to the corresponding spectral characteristics: mass spectra, accurate mass and characteristic fragmentation.

3 Results and Discussion

3.1 The Characterization of Synthesized nZVI

TEM analysis confirmed that synthesized iron particles are in the nano domain (Fig. 1). The majority of the particles, having diameter between 5 and 45 nm, possess approximately spherical shape and exist in close contact with each other which can be attributed to the magnetic properties of iron species [26].

According to SEM analysis, the nZVI sample consists of particles of a very wide range of sizes, from 70 nm to several tens of microns. These particles of different, mostly irregular shapes represent aggregates of nanoparticles, previously observed by TEM (Fig. 2a and 2b). The tendency of nZVI towards agglomeration in the aquatic environment is also mentioned in the literature as one of the main shortcomings
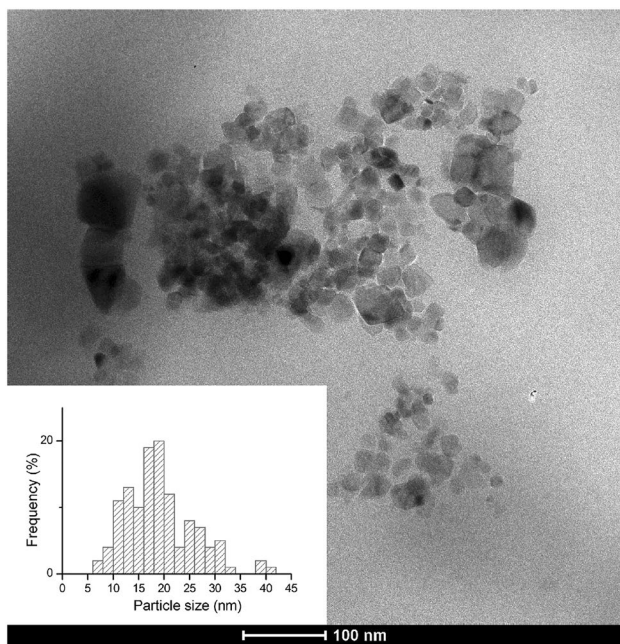
Fig. 1 TEM image of nZVI (inset: particle size distribution)

of this form of iron [27]. Unlike the conventional chemical method for nZVI synthesis, which mainly produces chain aggregates, in the case of green synthesis, the resulting aggregates can be of different shapes—cloud shapes, network aggregates, etc. [18]. The method of aggregation depends on the conditions of synthesis, but it is primarily determined by the type of plant extract used, i.e. its chemical composition. The results of the SEM analysis indicate that the synthesized sample of nZVI consists of a combination of different forms of aggregates, as a consequence of the heterogeneous composition of the used green tea extract.

In order to determine the surface chemical composition of the synthesized nZVI sample, an elementary analysis was performed by the EDS method. Figure 2c shows the EDS spectrum of one selected sample location with identified peaks of C, O, K and Fe. The elemental surface composition of the sample expressed by the mass fraction of the detected elements was: 44.06 wt% C, 33.37 wt% O, 2.74 wt% K and 19.83 wt% Fe. The C and O present are derived from polyphenolic groups and other organic compounds from the green tea extract. Also, the present K is of plant origin, since it is one of the very important elements for plant growth and is found in every living plant cell [28]. Therefore, based on the obtained results, it can be concluded that the surface of the tested nZVI sample is covered with organic compounds
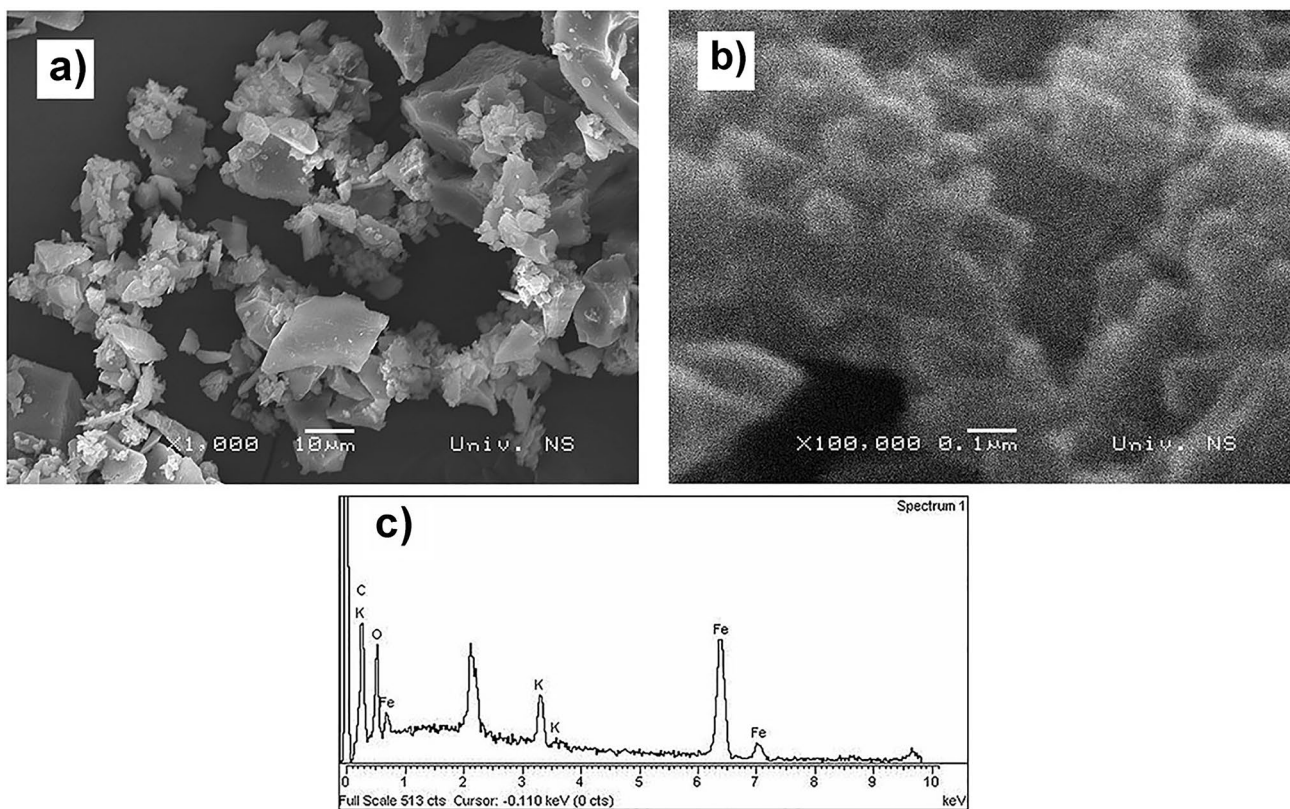

Fig. 2 SEM images of nZVI at **a** ×1000 and **b** ×100,000 magnification and **c** EDS spectrum of nZVI

originating from the green tea. Consequently, iron content appears quite low in the elemental analysis (19.83 wt%) because iron residing under carbon and oxygen cannot be measured by EDS analysis. The similar values of iron content in the green synthesized nZVI, obtained by EDS analysis, are reported by many other authors [17, 25, 28].

The ZetaSizer was used to determine the size distribution of nZVI aggregates. In this case, it should be noted that this method is based on the approximation of the spherical shape of the particles. As can be seen from the diagram shown in Fig. 3, the size of aggregates in the analyzed sample is in a very wide range of 80–6000 nm, with a diameter distribution characterized by two peaks, the first in the range of 80–600 nm with a maximum at 349 nm and the other from 600 to 3500 nm with a maximum at 1609 nm. The formation of the third peak is interrupted, since the maximum particle diameter that can be measured on this instrument is 6 μm. Therefore, it can be concluded that the tested sample also contains larger aggregates in the micro domain which is in accordance with the results of the SEM analysis.

The dried nZVI sample was analyzed by the X-ray diffraction method and the obtained diffractogram is shown in Figure S1. The synthesized nZVI is of amorphous character, since the presence of no characteristic iron peak was observed. The crystal structure of nZVI (α-Fe) is characterized by diffraction signals at values of 2θ of 44.68°, 65.03° and 82.35° with the corresponding Miller indices (110), (200) and (211), respectively (COD database code: 9008536, Reference code 96-900-8537) and has been identified by several authors in the case of obtaining nZVI by the method of green synthesis [19, 29, 30]. However, according to the results of most authors, the application of this method mainly results in nZVI of amorphous nature [31–33]. It is precisely this property that distinguishes green nZVI from that obtained by the classical method of chemical reduction using sodium borohydride [34, 35]. It can be assumed that the amorphous character of green nZVI is due to the heterogeneous composition of plant extracts used as a reducing

agent, or, in this case, green tea whose organic matter is seen on the diffractogram as a wide peak in the range 2θ from 20° to 25° [36].

N_2 adsorption–desorption isotherm of nZVI (inset of Figure S2) is typical of type IV with H3 hysteresis loop, originating from the slit-shaped mesopores [37]. The sample possesses exceptionally low specific surface area (1.04 m^2/g) and total pore volume (0.0025 cm^3/g), while the pore size distribution profile, with average pore diameter of 16.5 nm (Figure S2) can be portrayed with several maxima. Namely, the present micropores and mesopores in a lower diameter range (2–20 nm) can be attributed to the space between the individual particles, while the larger mesopores and detected macropores (dominant fraction) are formed between the nZVI aggregates.

3.2 The Determination of the Concentration of Synthesized nZVI in the Green Tea Extract

The efficiency of the selected method of Fe^{3+} reduction was determined by measuring the concentration of residual Fe^{3+} in the green tea extract after the completion of the synthesis. The concentration of residual (unreduced) Fe^{3+} was determined by UV–VIS spectrophotometry and is based on the formation of a purple Fe^{3+} complex with salicylic acid. The resulting complex has a maximum absorption in the visible region of the spectrum at a wavelength of $\lambda = 526.5$ nm. Taking into account the initial concentration and volume of the $Fe(NO_3)_3 \cdot 9H_2O$ solution as a precursor, the stoichiometric weight of Fe^0 obtained under the given conditions is 140 mg. The concentration of the residual Fe^{3+} in the green tea extract was determined on the basis of a previously made calibration curve for the Fe^{3+} complex with salicylic acid, and the calculated weight of the obtained Fe^0 is 125.8 mg. It follows that 89.85% of Fe^{3+} is reduced to Fe^0. This data on the obtained weight of Fe^0 was then used to calculate the concentration of nZVI in the green tea extract after the synthesis was completed:
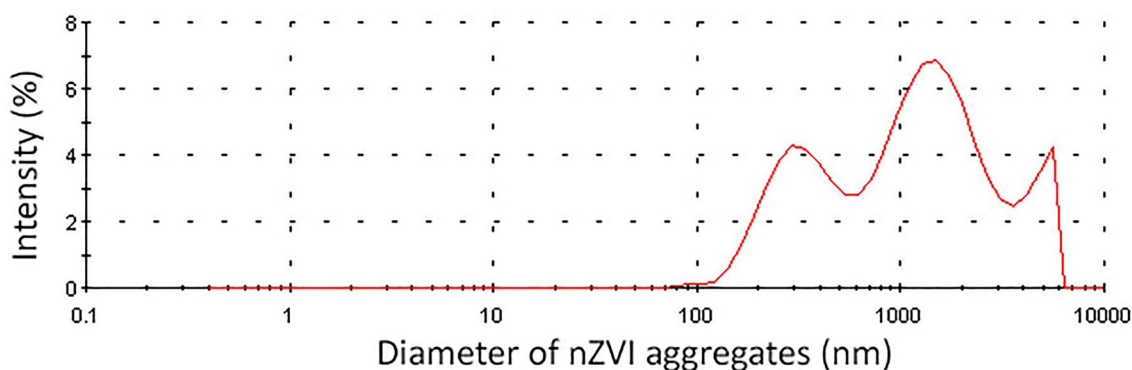

Fig. 3 Size distribution of nZVI aggregates

$$c\left(Fe^0\right) = \frac{m\left(\text{synthesized } Fe^0\right)}{V(\text{total volume of green tea extract after the synthesis})}$$

$$= \frac{1258 \text{ mg}}{125 \text{ ml}} = 10064 \frac{\text{mg}}{\text{ml}} \tag{1}$$

The calculated Fe^0 concentration was further used in the calculation of the nZVI concentration in the dye solution in the Fenton-like test reaction.

3.3 The Application of Synthesized nZVI in the Process of Textile Dye Degradation

3.3.1 The Effect of Homogenization Method

In order to determine the influence of the method of homogenization of methylene blue (MB) solution on the process efficiency, the reaction was performed on a magnetic stirrer (700 rpm), and in an ultrasonic bath (sonolysis). Other experimental conditions were identical in both processes: the initial concentration of MB 100 ppm solution, volume of MB 100 ml solution, nZVI concentration 2 ppm and H_2O_2 concentration of 600 ppm. No pH correction was performed during the process, and the measured pH values were identical in both tested systems. The initial pH value of the MB solution was 5.52. After the addition of nZVI and H_2O_2, the pH value decreased to 2.92, followed by its slight drop (2.75) by the end of the process (after 100 min). The decrease of the pH value is the consequence of the addition of higher dosage of H_2O_2 (600 ppm) using commercially available 30% H_2O_2 solution of low pH value. The presence of an acidic medium (pH < 4) is necessary in this process for the efficient formation of ·OH radicals. It is assumed that at pH > 4 the formation of these radicals is significantly slowed down due to the formation of ferri-hydroxy complexes, and thus the efficiency of the Fenton process [38] is significantly reduced. Based on the results, it can be concluded that the measured pH values are in the satisfactory range, there is no need for additional adjustment of pH values and they do not depend on the applied method of homogenization. Figure 4 shows the change in the concentration of the MB solution during 100 min of the process on a magnetic stirrer and in an ultrasonic bath.

As can be seen from Fig. 4, the use of ultrasound slightly increases the efficiency of MB degradation, which is 97.60% at the end of the process (after 100 min), while in the process of homogenization by magnetic stirring, 92.24% of this dye is removed. The largest difference in the rate of these two processes can be noticed during the first 20 min of the reaction, after which, in both cases, equilibrium is gradually established. Ultrasonic treatment removes 85.01% of MB during the first 3 min of the process, while this percentage in the case of magnetic homogenization is 51.79%. The presented results clearly indicate the positive effect of
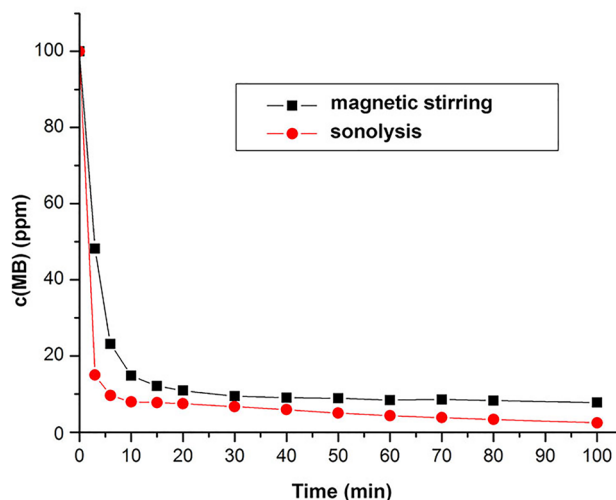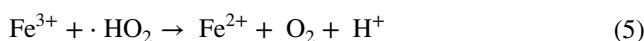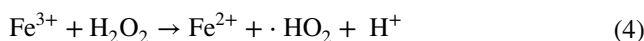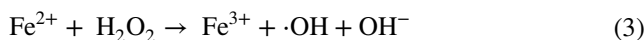

Fig. 4 The effect of the homogenization method on the efficiency of MB degradation process
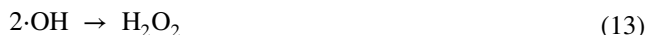
ultrasound, but only at the beginning of the process, mainly as the consequence of the mechanism of the Fenton reaction [39]. In the case of using Fe^0 as a catalyst, this mechanism is based on the corrosion (oxidation) of nZVI to Fe^{2+} ions, which further react with H_2O_2. The use of ultrasound stimulates the production of Fe^{2+} ions, which is one of the aspects of its positive effect (Eqs. 2–5):

$$Fe^0 + UZ \rightarrow Fe^{2+} + 2e^- \tag{2}$$

$$Fe^{2+} + H_2O_2 \rightarrow Fe^{3+} + \cdot OH + OH^- \tag{3}$$

$$Fe^{3+} + H_2O_2 \rightarrow Fe^{2+} + \cdot HO_2 + H^+ \tag{4}$$

$$Fe^{3+} + \cdot HO_2 \rightarrow Fe^{2+} + O_2 + H^+ \tag{5}$$

Another aspect is reflected in the increased production of ·OH radicals that further play a key role in dye degradation (Eqs. 6–9):

$$H_2O_2 + UZ \rightarrow 2 \cdot OH \tag{6}$$

$$O_2 + UZ \rightarrow 2O \cdot \tag{7}$$

$$O \cdot + H_2O \rightarrow 2 \cdot OH \tag{8}$$

$$\cdot OH + \cdot OH \rightarrow H_2O_2 \tag{9}$$

Also, by the sonolysis of water molecules, a small amount of ·OH radicals can be formed, which, by further recombination, give an additional amount of H_2O_2 (Eqs. 10–13) [40, 41]:

$$H_2O + UZ \rightarrow \cdot OH + \cdot H \tag{10}$$

$$\cdot H + O_2 \rightarrow \cdot HO_2 \tag{11}$$

$$2 \cdot HO_2 \rightarrow H_2O_2 + O_2 \tag{12}$$

$$2 \cdot OH \rightarrow H_2O_2 \tag{13}$$

It can be assumed that the proposed mechanism is valid in the specific case of MB degradation under the previously mentioned experimental conditions. The oxidation of Fe^0 is supported by the presence of an acidic environment, as well as the use of ultrasound, resulting in an increased concentration of Fe^{2+} and $\cdot OH$ radicals, which increases the efficiency of dye degradation in the first minutes of the process.

3.3.2 The Effect of the nZVI Concentration

In order to investigate the influence of the nZVI concentration on the efficiency of MB degradation, sonolysis was performed at two constant H_2O_2 concentrations (100 ppm and 600 ppm), while the nZVI concentration was varied in the range of 0–20 ppm (Fig. 5). In the case of H_2O_2 concentration of 100 ppm, in the absence of nZVI, the percentage of dye removal from the solution was only 5.78%. By providing only 2 ppm of nZVI, the oxidative degradation process is significantly accelerated, with most of the dye being removed during the first 30 min of the process (78.22%). By further increasing the concentration of nZVI, almost the entire amount of dye is removed during the first 10 (90.64%) and 3 min of the process (90.87%), at nZVI concentrations of 6 and 10 ppm, respectively. The present catalyst concentration of 20 ppm showed a negative impact on the

efficiency of the process (the percentage of the MB removal was 88.83% after 100 min). Therefore, there is a limit value (6 ppm) above which excess nZVI has only a slight impact on the further course of dye degradation, while its further increase (> 10 ppm) reduces the process efficiency. This phenomenon can be attributed to the mechanism of the Fenton reaction. Namely, by increasing the concentration of nZVI, under ultrasound, a larger amount of Fe^{2+} ions is formed, which then initiates the decomposition of H_2O_2 to hydroxyl radicals. In case a large amount of these radicals is formed in a short time, in addition to reacting with dye molecules, they can also participate in a side, unwanted reaction, which is the mentioned effect of removing $\cdot OH$ radicals. This way, the process of dye degradation is not improved, but is rather inhibited (Eq. 14) [28].

$$Fe^{2+} + \cdot OH \rightarrow Fe^{3+} + OH^- \tag{14}$$

Six times higher H_2O_2 concentration results in a very fast sonolysis process, even at the lowest nZVI concentration of 2 ppm. Almost the entire amount of MB is removed during the first 3 min of the process (> 97%), regardless of the amount of nZVI present. The maximum efficiency of dye removal was achieved in the presence of 10 ppm nZVI and was 99.37% after 100 min of the sono-process.

3.3.3 The Effect of the H_2O_2 Concentration

Figure 6 shows the effect of H_2O_2 concentration (0–600 ppm) on the efficiency of the MB degradation process at nZVI concentration of 10 ppm. As can be seen from the diagram the efficiency of dye removal increases with increasing H_2O_2 concentration. Regardless of the applied concentration of
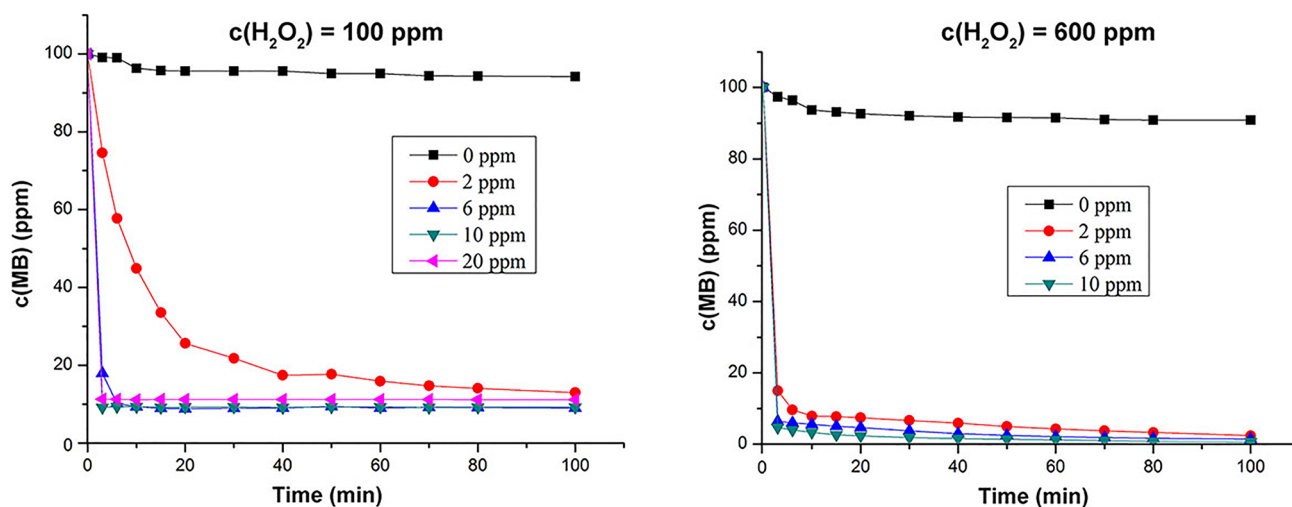

Fig. 5 The effect of the nZVI concentration on the efficiency of MB degradation process
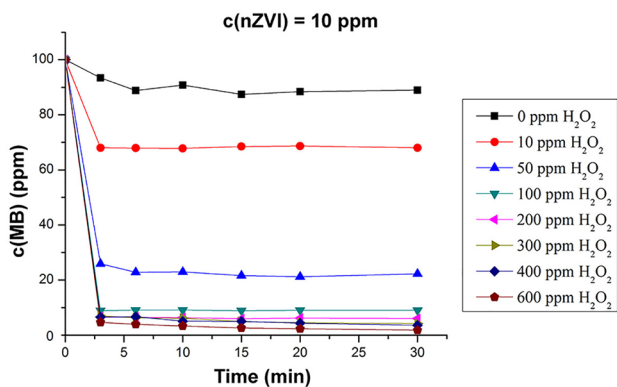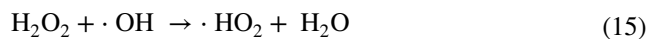
Fig. 6 The effect of the H_2O_2 concentration on the efficiency of MB degradation process

$$H_2O_2 + \cdot OH \rightarrow \cdot HO_2 + H_2O \qquad (15)$$

3.3.4 The Proposed Degradation Mechanism of the Tested Dyes

The previously presented results of the process optimization showed that the highest efficiency of the MB degradation is achieved at nZVI concentration of 10 ppm and H_2O_2 of 600 ppm. For these experimental conditions, Fig. 7 shows the decrease in the intensity of the absorption peaks on the UV–VIS spectrum of the MB solution during sonolysis. The interruption in the spectrum of the initial solution with an MB concentration of 100 ppm was caused by the upper limit of detection of the used UV–VIS spectrophotometer (absorbance = 3).

The UV–VIS spectrum of MB solution is characterized by one absorption maximum in the UV region of the spectrum at a wavelength of $\lambda = 292$ nm which can be attributed to the presence of benzene rings in the structure of molecules. The second absorption maximum in the visible region of the spectrum at a wavelength of $\lambda = 664$ nm originates from heteropolyaromatic bonds in the molecule, which are constituents of the chromophore as a color carrier [40]. As can be seen from Fig. 7, during the process there is a change in the intensity of absorption peaks, which is the result of structural changes within MB molecules. The intensity of the absorption peak at 664 nm decreases sharply after only 3 min of sonolysis indicating the destruction of the part of the molecule responsible for the presence of blue color. As a result, the color of the solution changes, and during the process, it becomes completely discolored. Also, after few

H_2O_2, the process takes place very quickly in the given experimental conditions, so that almost the entire amount of MB is removed during the first 3 min of the process. By increasing the H_2O_2 concentration above 100 ppm, the degree of MB degradation achieved after 30 min of reaction varies in a very narrow range—from 90.96 to 98.17% for concentrations from 100 to 600 ppm, respectively. Based on the presented results, it can be concluded that, as in the case of nZVI concentration, there is a limit value (100 ppm) for H_2O_2 concentration above which no significantly higher process efficiency is achieved, which is again a consequence of the unwanted removal of ·OH radicals (Eq. 15) [42]. Hydroperoxy radicals (·HO_2) formed in this process have significantly less activity compared to ·OH radicals. Therefore, the mentioned concentration can be considered optimal from the point of view of process economy, regardless of the somewhat lower efficiency achieved.

Fig. 7 The reduction of the intensity of absorption peaks on the UV–VIS spectrum of the MB solution during sonolysis (inset: the basic spectrum of the MB solution)
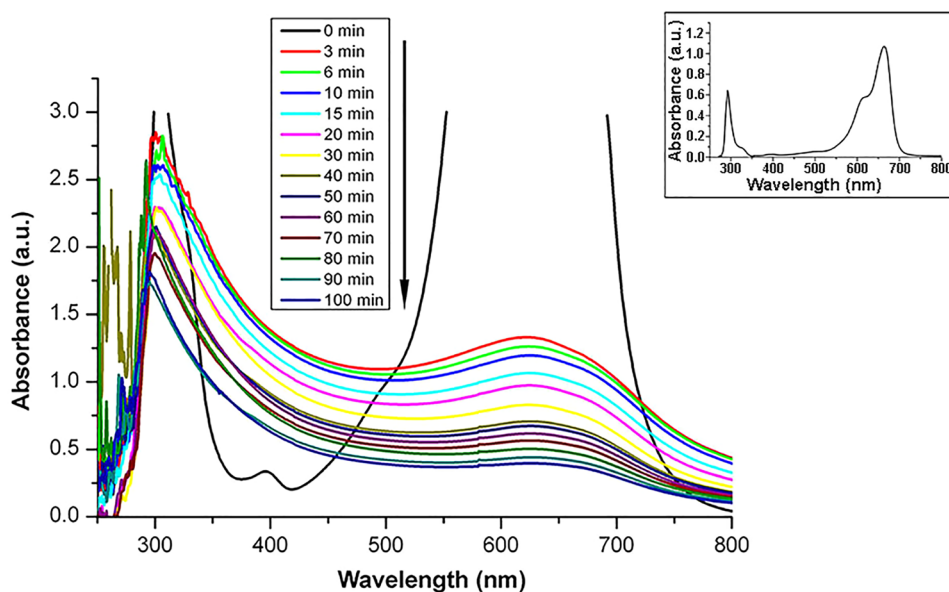
minutes of the reaction the absorption maximum in the visible region of the spectrum shifts from 664 to 620 nm which is the so-called blue shift and is mainly associated with dye aggregation in an acidic medium [33]. The formation of the blue shift has been noted in the literature in the base environment, and it is assumed that originates from the demethylation of MB molecules, rather than from their aggregation [43]. Since the measured pH values during the examined process indicate the presence of an acidic environment, it can be suggested that the aggregation of dye molecules causes the mentioned shift. During sonolysis, the intensity of the absorption maximum in the UV region of the spectrum decreases and this decrease is much smaller and more gradual in relation to the absorption maximum in the visible region. The presence of a given peak even after 100 min of sonolysis indicates that some degradation product(s) containing aromatic molecular structure is/are still present in the solution. The degradation mechanism of methyl orange (MO) and bromothymol blue (BTB) was considered at the same values of process parameters as for MB: nZVI and H_2O_2 concentrations of 10 ppm and 600 ppm, respectively. The pH value of the MO solution was 3.50 at the beginning of the reaction (after the addition of nZVI and H_2O_2), and 2.76 at the end (after 100 min), while the corresponding pH values of the BTB solution were 3.30 and 2.82. Therefore, as in the case of MB degradation, the measured pH values are in a satisfactory range and no additional correction is required. Figure 8 shows the decrease in absorption intensity on the UV–VIS spectrum of these two dyes during the reaction.

Unlike MB, whose degradation under the same experimental conditions is almost instantaneous (95.3% is decomposed during the first 3 min of the process), the degradation

of MO is a slower process, with the same percentage of removal achieved after 15 min of reaction (Fig. 8a). The efficiency of sonolysis at the end of the reaction is 98.8%. In the case of BTB degradation (Fig. 8b), 88.6% of this dye is removed by the end of the process. Compared to MO, the BTB sonolysis is characterized by lower rate, with the degradation of most of the dye (85.4%) taking 40 min. Further progress of the reaction removes an additional 3.2%. The MO spectrum is characterized by two absorption maxima, one in the UV region at a wavelength of $\lambda = 292$ nm, while the other is in the visible region of the spectrum at a wavelength of $\lambda = 465$ nm. As in the case of MB, the peak in the UV region of the spectrum is due to the presence of benzene rings in the structure of molecules, while the peak in the visible region originates from a conjugated structure with an azo group, which forms a molecular chromophore and gives color [44]. After 3 min of the reaction, the peak intensity at 465 nm was considerably reduced (Fig. 8a). The Fenton mechanism of dye degradation is based on the reaction between dye molecules and ·OH radicals. In the case of MO, the azo bond first reacts with ·OH radicals, which causes the loss of chromophore characteristics of MO [45]. Since there are no newly formed peaks in the visible region of the spectrum, it can be suggested that the breaking of the azo bond resulted in particular intermediates that do not absorb light in this region of the spectrum. The degradation of the aromatic parts of MO molecules occurs much more slowly and gradually, and the presence of peaks in the UV region at the end of the process indicates that some degradation product(s) with aromatic molecular structure is/are still present in the solution.

The BTB degradation process was also monitored by recording the absorption spectrum of the solution during
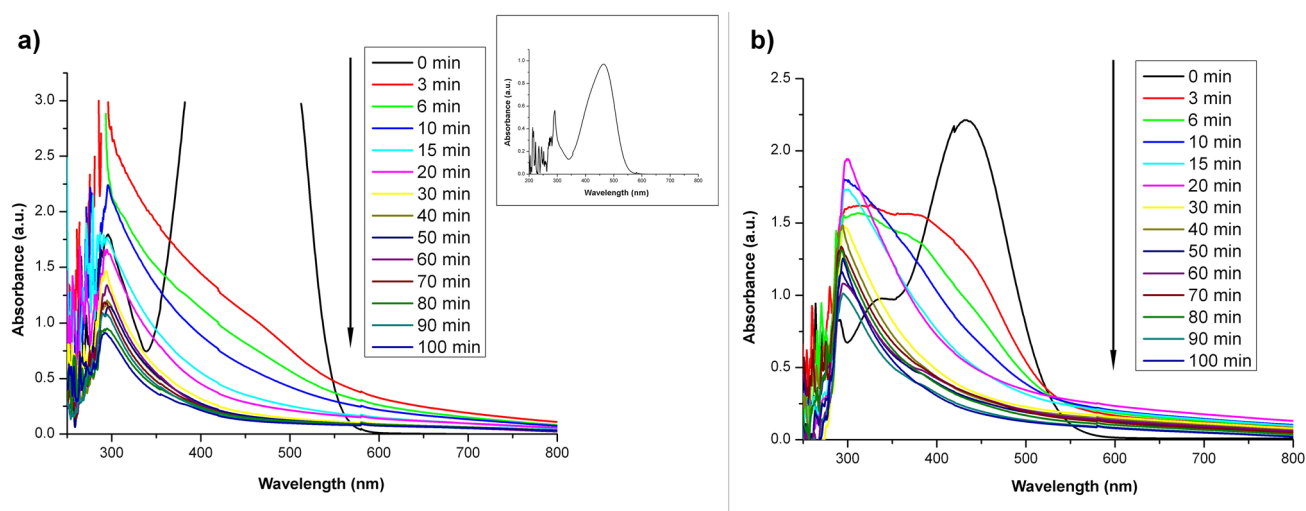

Fig. 8 The reduction of the intensity of absorption peaks on the UV–VIS spectrum of: **a** MO solution (inset: the basic spectrum of the MO solution) and **b** BTB solution during sonolysis

100 min of the reaction (Fig. 8b). As can be seen from the figure shown, the BTB solution has three absorption maxima, two in the UV region at wavelengths of 290 nm and 340 nm, and one in the visible region of the spectrum at 435 nm. After only 3 min of sonolysis, the intensity of absorption in the visible region of the spectrum decreases which is accompanied by a gradual loss of color of the solution, while the intensity of peaks in the UV region initially increases during 20 min and then gradually decreases until the end of the process. The BTB molecule contains three benzene rings in its structure, so it can be assumed that the degradation (transformation) of this structure firstly produces some aromatic product(s) that absorb light in the UV region of the spectrum, and thus the intensity of peaks in this region increases. After 20 min of the process, the gradual degradation (transformation) of these aromatic intermediates begins and it is not completed until the end of the reaction.

3.3.5 Determination of the Degradation Products of the Tested Dyes

The degradation products of the three tested dyes were identified using UHPLC-DAD-ESI-MS/MS analysis. Figures S3–S5 represent the total mass chromatograms of the solutions of methylene blue, methyl orange and bromothymol blue being degraded for 100 min (end of the Fenton-like process). The list of the identified compounds in the resulting solutions of all three dyes is given in Tables S2–S4. The molecule of methylene blue provides a signal corresponding to a positive ion at m/z 284.18, with three significant m/z values on MS/MS spectrum: 239.84, 241.20 and 267.8. At the end of Fenton-like process, one product was identified in the resulting solution—leuco-methylene blue (LMB) with a peak at m/z 286.11 with four fragment ions on MS/MS spectrum at m/z values: 228.02, 242.51, 255.7 and 270.0. Considering the intensities of the peaks assigned to MB and LMB (Figure S3), it can be suggested that almost entire amount of MB present in the initial solution was converted to LBM. This transformation pathway includes the oxidation of nZVI, followed by the emission of two electrons responsible for the change of MB to colorless LMB [46]. In the case of MO, the appropriate chromatogram of the resulting solution contains four peaks (Figure S4)—peak at m/z 304.06 originating from the unreacted (residual) MO amount and three peaks of low intensities at m/z values: 320.11, 290.16 and 276.21. The characteristic peak of MO at m/z 304.06 derives from the negative ion of the MO dye $[M–H]^-$, while its MS/MS spectrum yields three product ions at m/z values: 289.04 (cleavage of one methyl group), 240.20 (cleavage of a sulfonate group) and 156.03 derived from $[M–H–N_2C_6H_4N(CH_3)_2]^-$ [47]. The appearance of the peak at m/z 320.11 is the consequence of the presence of mono-hydroxylated product of MO characterized by three fragment

ions at MS/MS spectrum at m/z values: 304.87 (MO), 255.94 ($[M–H–SO_2]^-$) and 155.96 ($[M–H–N_2C_6H_3(OH)N(CH_3)_2]^-$) [48]. The signal at m/z 290.16 can be attributed to a degradation product formed after MO loses one methyl group. This peak reveals three fragment ions at MS/MS spectrum at m/z values: 275 ($[M–H–CH_3]^-$), 226 ($[M–H–SO_2]^-$) and 156 ($[M–H–N_2C_6H_4NHCH_3]^-$) [48]. Additionally, the fourth peak present at m/z 276.21 originates from the degradation product of demethylation reaction (obtained by replacement of two methyl groups in MO molecule by hydrogen atoms). The corresponding fragment ions of this peak at MS/MS spectrum are at m/z values: 212 ($M–H–SO_2]^-$) and 156 ($[M–H–N_2C_6H_4NH_2]^-$) [48]. By comparing the obtained intensities of the peaks derived from the initial solution (not shown) and the resulting one, it can be suggested that the parent MO molecule scarcely exists in the solution after the degradation process along with other three identified products. Furthermore, the recorded degradation products are present in very low amounts (trace levels) indicating that most of the MO dye present in the initial solution was completely mineralized into CO_2 and water. The chromatogram obtained from the solution of bromothymol blue after degradation is portrayed by four peaks (Figure S5)—peak at m/z 625 (with 7 fragment ions on MS/MS spectrum) originating from the residual BTB amount in the solution and three peaks at m/z values: 623, 739 and 593. The compound at m/z value 623 with appropriate products ions was identified as ketobromothymol blue, while the other two degradation products remained unknown and characterized only by their fragment ions on MS/MS spectrum. Based on the intensities of the peaks obtained from the initial solution (not shown) and the resulting one, it can be presumed that the BTB molecules were mineralized to quite high extent to CO_2 and water after 100 min of process, leaving some trace amounts of the parent BTB, ketobromothymol blue and one product with m/z value 593, while the unidentified compound with m/z value 739 is still present in the solution at slightly higher level.

3.3.6 Kinetic Study

In order to study the degradation kinetics of the particular textile dyes in heterogeneous Fenton-like oxidation under different conditions, four kinetic models were used to fit the experimental data. The kinetic parameters were calculated by the linear regression analyses of c_t versus t for the zero-order (ZO) model, $ln(c_0/c_t)$ versus t for the first order (FO) model, $[(1/c_t) − (1/c_0)]$ versus t for the second order (SO) model and $t/[1 − (c/c_0)]$ versus t for the Behnajady-Modirshahla-Ghanbery model (BMG) [49]. Two constants in BMG model, m (min) and b (dimensionless), are related to initial reaction rate and oxidation capacity, respectively. They are evaluated by examining the time approaching zero or infinity, consequently

leading to the initial dye degradation rate (1/m) and maximum theoretical conversion that could have been achieved after a very long or infinite reaction time (1/b), hence named as the maximum oxidation capacity [49, 50]. Accordingly, higher values of 1/m and 1/b indicate better catalytic performance [51]. Linear equations for all models and denotation of parameters are given in Table S1, while the fitting results are presented in Table 1. According to the kinetic data, the correlation coefficients (R^2) were in a very wide range. Very low values obtained in the case of ZO model for all studied experimental data indicate an inadequate fitting, while on the other hand, the BMG model proved to be the best for the description of kinetics of all tested processes. Considering the effect of homogenization method, besides the BMG model, which fitted best to the data in both processes—magnetic stirring and sonolysis ($R^2 = 0.9998$ in both cases), only SO model in the case of MB sonolysis can be considered as partially adequate with the rate constant of $k_2 = 0.003 \, l \, mg^{-1} \, min^{-1}$. By analyzing the parameters 1/m and 1/b obtained by the BMG model of these two processes, it is possible to observe a slightly positive effect of ultrasound reflected by the higher value of initial degradation rate. On the other hand, the maximum oxidation capacities under different homogenization treatments are almost the same. After increasing the nZVI concentration to 10 ppm, the BMG model is still the most adequate to describe the MB degradation kinetics with the value of initial degradation rate three times higher compared to the process with the nZVI concentration of 2 ppm. This also coincides with the k_2 value being substantially higher ($k_2 = 0.013 \, l \, mg^{-1} \, min^{-1}$), if SO model can be considered as the one following the BMG model based on the experimental data fitting suitability. Regarding the appropriate parameters of BMG model for the degradation of additional two textile dyes (MO and BTB), it can be suggested that their initial degradation rates are quite lower compared to the MB degradation under the same reaction conditions, while the oxidation capacities are similar regardless of the type of the degraded dye. Other kinetic models cannot be applied to describe the Fenton-like oxidation of MO and BTB under these specified reaction parameters. The presented kinetic results indicate that the degradation process of the examined dyes proceeds via two stages (two-stage pattern)—a fast one and a much slower one [50], regardless of the used reaction conditions. Hence, it could not be modeled by ZO, FO and SO reaction kinetics, proposing the BMG model as the best representing this system kinetics.

4 Conclusions

The applied green synthesis of zero-valent iron using the green tea extract as a reducing agent provided amorphous, approximately spherical nanoparticles with diameter between 5 and 45 nm with high tendency to form

Table 1 Degradation kinetic parameters

Textile dye	Concentration		Homogenization method	ZO model		FO model		SO model		BMG model		
	nZVI (ppm)	H_2O_2 (ppm)		R^2	k_0 (mg l^{-1} min^{-1})	R^2	k_1 (min^{-1})	R^2	k_2 (l mg^{-1} min^{-1})	R^2	1/m (min^{-1})	1/b
MB	2	600	magnetic stirring	0.2778	0.213	0.4766	0.012	0.6764	0.0009	0.9998	0.729	0.934
MB	2	600	sonolysis	0.7162	0.092	0.9285	0.015	0.9497	0.0030	0.9998	1.043	0.977
MB	10	600	sonolysis	0.7806	0.037	0.9564	0.019	0.9716	0.013	0.9999	3.125	0.995
MO	10	600	sonolysis	0.3686	0.123	0.6598	0.024	0.8269	0.0082	0.9999	1.602	0.995
BTB	10	600	sonolysis	0.7140	0.275	0.8223	0.013	0.9019	0.0007	0.9997	0.322	0.909

Reaction conditions: c_0(textile dye) = 100 ppm; V(textile dye) = 100 ml

aggregates of different shapes and size (from 70 nm to several tens of μm). In addition to Fe as the preferred active phase of the catalyst, the synthesized nZVI also contains elements originating from the organic compounds present in the green tea (C, O and K). The sample possesses exceptionally low specific surface area ($1.04 \ m^2/g$) and total pore volume ($0.0025 \ cm^3/g$), followed by a diverse pore size distribution—the present micropores and mesopores in a lower diameter range (2–20 nm) can be attributed to the space between the individual particles, while the larger mesopores and detected macropores (dominant fraction) are formed between the nZVI aggregates. The results of MB degradation in the presence of nZVI indicate a slightly positive effect of ultrasound on the process efficiency in relation to the magnetic stirring, but only at the beginning of the process. The optimization of nZVI concentration has established the existence of a certain limit value (6 ppm) (at H_2O_2 concentration of 100 ppm) above which excess nZVI has insignificant impact on the further course of dye degradation, while its further increase (> 10 ppm) reduces the process efficiency. By increasing the concentration of H_2O_2, both the rate and efficiency of MB removal increases, leading to another limit value (100 ppm) above which no significantly higher process efficiency is achieved. Based on the obtained individual UV–VIS spectra for the tested dyes, as well as the identified products at the end of the process, degradation mechanism for each dye has been proposed, suggesting that the corresponding part of the molecule—the chromophore, as a color carrier, is almost completely degraded in all three dyes, but some aromatic compounds absorbing the light in UV region are still present in the solution after the reaction. Kinetic data have proved that the BMG model is the best for the description of kinetics of all tested processes indicating that the degradation process of the examined dyes proceeds via two stages (two-stage pattern)—a fast one and a much slower one. The reactions can be portrayed by notably different initial degradation rates, but the appropriate maximum oxidation capacities are quite similar.

Declarations

Competing interests The authors declare that they have no known competing financial interests or personal relationships that could have appeared to influence the work reported in this paper.

References

1. Galdames A, Ruiz-Rubio L, Orueta M, Sánchez-Arzalluz M, Vilas-Vilela JL (2020) Zero-valent iron nanoparticles for soil and groundwater remediation. Int J Environ Res Public Health 17:5817

2. Crane RA, Scott TB (2012) Nanoscale zero-valent iron: future prospects for an emerging water treatment technology. J Hazard Mater 211–212:112–125

3. Lye JWP, Saman N, Noor AMM, Mohtar SS, Othman NS, Sharuddin SSN, Kong H, Mat H (2020) Application of nanoscale zero-valent iron-loaded natural zeolite for tetracycline removal process. Chem Eng Technol 43(7):1285–1296

4. Mondal P, Anweshan A, Purkait MK (2020) Green synthesis and environmental application of iron-based nanomaterials and nanocomposite: a review. Chemosphere 259:127509

5. Le NT, Dang T-D, Binh KH, Nguyen TM, Xuan TN, La DD, Nadda AK, Chang SW, Nguyen DD (2022) Green synthesis of highly stable zero-valent iron nanoparticles for organic dye treatment using Cleistocalyxoperculatus leaf extract. Sustain Chem Pharm 25:100598

6. Liang L, Tan W, Xue Y, Xi F, Meng X, Hu B, Du J (2022) Effects of magnetic field on selenite removal by sulfidated zero valent iron under aerobic conditions. Sci Total Environ 831:154755

7. Wang CB, Zhang WX (1997) Synthesizing nanoscale iron particles for rapid and complete dechlorination of TCE and PCBs. Environ Sci Technol 31:2154–2156

8. O'Caroll D, Sleep B, Krol M, Boparai H, Kocur C (2013) Nanoscale zero-valent iron and bimetallic particles for contaminated site remediation. Adv Water Res 51:104–122

9. Ravikumar KVG, Dubey S, Chandrasekaran N, Mukherjee A (2016) Scale-up synthesis of zero-valent iron nanoparticles and their applications for synergistic degradation of pollutants with sodium borohydride. J Mol Liq 224:589–598

10. Danila V, Vasarevicius S, Valskys V (2018) Batch removal of Cd(II), Cu(II), Ni(II), and Pb(II) ions using stabilized zero-valent iron nanoparticles. Energy Proc 147:214–219

11. Zhou N, Gong K, Hu Q, Cheng X, Zhou J, Dong M, Wang N, Ding T, Qiu B, Guo Z (2020) Optimizing nanocarbon shell in zero-valent iron nanoparticles for improved electron utilization in Cr(VI) reduction. Chemosphere 242:125235

12. Fu F, Dionysiou DD, Liu H (2014) The use of zero-valent iron for groundwater remediation and wastewater treatment: a review. J Hazard Mater 267:194–205

13. Stefaniuk M, Oleszczuk P, Ok YS (2016) Review on nano zero-valent iron (nZVI): from synthesis to environmental applications. Chem Eng J 287:618–632

14. Machado S, Stawiński W, Slonina P, Pinto AR, Grosso JP, Nouws HPA, Albergaria JT, Delerue-Matos C (2013) Application of green zero-valent iron nanoparticles to the remediation of soils contaminated with ibuprofen. Sci Total Environ 461–462:323–329

15. Demirezen DA, Yildtz YS, Yilmaz S, Yilmaz D (2019) Green synthesis and characterization of iron oxide nanoparticles using Ficuscarica (common fig) dried fruit extract. J Biosci Bioeng 127:241–245

16. Karpagavinayagam P, Vedhi C (2019) Green synthesis of iron oxide nanoparticles using *Avicennia marina* flower extract. Vacuum 160:286–292

17. Mareedu T, Poiba VR, Vangalapati M (2021) Green synthesis of iron nanoparticles by green tea and black tea leaves extract. Mater Today Proc 42:1498–1501

18. Machado S, Pacheco JG, Nouws HPA, Albergaria JT, Delerue-Matos C (2013) Characterization of green zero-valent iron nanoparticles produced with tree leaf extracts. Sci Total Environ 533:76–81

19. Hoag GE, Collins JB, Holcomb JL, Hoag JR, Nadagouda MN, Varma RS (2009) Degradation of bromothymol blue by 'greener' nanoscale zero-valent iron synthesized using tea polyphenols. J Mater Chem 19:8671–8677

20. Babuponnusami A, Muthukumar K (2014) A review on Fenton and improvements to the Fenton process for wastewater treatment. J Environ Chem Eng 2:557–572

21. Maroudas A, Pandis PK, Chatzopoulou A, Davellas L-R, Sourkouni G, Argirusis C (2021) Synergetic decolorization of azo dyes using ultrasounds, photocatalysis and photo-fenton reaction. Ultrason Sonochem 71:105367

22. Wang N, Zheng T, Zhang G, Wang P (2016) A review on Fenton-like processes for organic wastewater treatment. J Environ Chem Eng 4:762–787

23. Genuino HC, Mazrui N, Seraji MS, Luo Z, Hoag GE (2013) Green synthesis of iron nanomaterials for oxidative catalysis of organic environmental pollutants. In: Suib SL (ed) New and future developments in catalysis. Elsevier, Amsterdam, pp 41–61

24. Raman CD, Konmani S (2016) Textile dye degradation using nano zero valent iron. J Environ Manag 177:341–355

25. Huang L, Weng X, Chen Z, Megharaj M, Naidu R (2014) Green synthesis of iron nanoparticles by various tea extracts: comparative study of the reactivity. Spectrochim Acta Part A 130:295–301

26. Wang X, Wang A, Ma J, Fu M (2017) Facile green synthesis of functional nanoscale zero-valent iron and studies of its activity toward ultrasound-enhanced decolorization of cationic dyes. Chemosphere 166:80–88

27. He Y, Gao J, Feng F, Liu C, Peng Y, Wang S (2012) The comparative study on the rapid decolorization of azo, anthraquinone and triphenylmethane dyes by zero-valent iron. Chem Eng J 179:8–18

28. Kuang Y, Wang Q, Chen Z, Megharaj M, Naidu R (2013) Heterogeneous Fenton-like oxidation of monochlorobenzene using green synthesis of iron nanoparticles. J Coll Inter Sci 410:67–73

29. Puiatti GA, de Carvalho JP, de Matos JP, Lopes RP (2022) Green synthesis of Fe^0 nanoparticles using *Eucalyptus grandis* leaf extract: characterization and application for dye degradation by a (Photo) Fenton-like process. J Environ Manag 311:114828

30. Jain R, Mendiratta S, Kumar L, Srivastava A (2021) Green synthesis of iron nanoparticles using Artocarpus heterophyllus peel extract and their application as a heterogeneous Fenton-like catalyst for the degradation of Fuchsin Basic dye. Curr Res Green Sustain Chem 4:100086

31. Truskewycz A, Shukla R, Ball AS (2016) Iron nanoparticles synthesized using green tea extracts for the fenton-like degradation of concentrated dye mixtures at elevated temperatures. J Environ Chem Eng 4:4409–4417

32. Njagi EC, Huang H, Stafford L, Genuino H, Galindo HM, Collins JB, Hoag GE, Suib SL (2011) Biosynthesis of iron and silver nanoparticles at room temperature using aqueous Sorghum bran extracts. Langmuir 27:264–271

33. Shahwan T, Sirriah SA, Nairat M, Boyac E, Eroğlu AE, Scott TB, Hallam KR (2011) Green synthesis of iron nanoparticles and their application as a Fenton-like catalyst for the degradation of aqueous cationic and anionic dyes. Chem Eng J 172:258–266

34. Arancibia-Miranda N, Baltazar SE, Garcia A, Romero AH, Rubio MA, Altbir D (2014) Lead removal by nano-scale zero valent iron: surface analysis and pH effect. Mater Res Bull 59:341–348

35. Zha SX, Cheng Y, Gao Y, Chen ZL, Megharaj M, Naidu R (2014) Nanoscale zerovalent iron as a catalyst for heterogeneous Fenton oxidation of amoxicillin. Chem Eng J 255:141–148

36. Wang T, Jin X, Chen Z, Megharaj M, Naidu R (2014) Green synthesis of Fe nanoparticles using eucalyptus leaf extracts for treatment of eutrophic wastewater. Sci Total Environ 466–467:210–213

37. Lowell S, Shields JE, Thomas MA, Thommes M (2004) Characterization of porous solids and powders: surface area, pore size and density, vol 16. Kluwer Academic Publishers, Dordrecht

38. Kuo WG (1992) Decolorizing dye wastewater with Fenton's reagent. Water Res 26:881–886

39. Lin J, Zhao X, Liu D, Yu Z, Zhang Y, Xu H (2008) The decoloration and mineralization of azo dye C.I. Acid Red 14 by sonochemical process: rate improvement *via* Fenton's reactions. J Hazard Mater 157:541–546

40. Weng C, Huang V (2015) Application of Fe^0 aggregate in ultrasound enhanced advanced Fenton process for decolorization of methylene blue. J Ind Eng Chem 28:153–160

41. Yuan N, Zhang G, Guo S, Wan Z (2016) Enhanced ultrasound-assisted degradation of methyl orange and metronidazole by rectorite-supported nanoscale zero-valent iron. Ultrason Sonochem 28:62–68

42. Weng C, Lin Y, Chang C, Liu N (2013) Decolourization of direct blue 15 by Fenton/ultrasonic process using a zero-valent iron aggregate catalyst. Ultrason Sonochem 20:970–977

43. Singhal GS, Rabinowitch E (1967) Changes in the absorption spectrum of methylene blue with pH. J Phys Chem 71:3347–3349

44. Fan J, Guo Y, Wang J, Fan M (2009) Rapid decolorization of azo dye methyl orange in aqueous solution by nanoscale zero-valent iron particles. J Hazard Mater 166:904–910

45. Dong H, Sans C, Li W, Qiang Z (2016) Promoted discoloration of methyl orange in H$_2$O$_2$/Fe(III) Fenton system: effects of gallic acid on iron cycling. Separ Purif Tech 171:144–150

46. Tarekegn MM, Balakrishnan RM, Hiruya AM, Dekeboa AH (2021) Removal of methylene blue dye using nano zerovalent iron, nanoclay and iron impregnated nanoclay—a comparative study. RSC Adv 11:30109

47. Holčapek M, Volná K, Vaněrková D (2007) Effects of functional groups on the fragmentation of dyes in electrospray and atmospheric pressure chemical ionization mass spectra. Dyes Pigm 75:156–165

48. Chen T, Zheng Y, Lin J-M, Chen G (2008) Study on the photocatalytic degradation of methyl orange in water using Ag/ZnO as catalyst by liquid chromatography electrospray ionization ion-trap mass spectrometry. J Am Soc Mass Spectrom 19:997–1003

49. Behnajady MA, Modirshahla N, Ghanbary F (2007) A kinetic model for the decolorization of C.I. Acid Yellow 23 by Fenton process. J Hazard Mater 148:98–102

50. Haji S, Khalaf M, Shukrallah M, Abdullah J, Ahmed S (2014) A kinetic comparative study of azo dye decolorization by catalytic wet peroxide oxidation using Fe–Y zeolite/H$_2$O$_2$ and photooxidation using UV/H$_2$O$_2$. React Kinet Mech Catal 114:795–815

51. Roumila Y, Meziani D, Debaghi S, Abdmeziem K (2021) Degradation of methyl violet over fenton-like hydroxyapatite catalysts, kinetics and thermodynamics studies. Res Square. https://doi.org/10.21203/rs.3.rs-569149/v1

Publisher's Note Springer Nature remains neutral with regard to jurisdictional claims in published maps and institutional affiliations.

Authors and Affiliations

Sanja Panić[1] · Mirjana Petronijević[1] · Jelena Vukmirović[1] · Nenad Grba[2] · Saša Savić[3]

✉ Nenad Grba
   nenad.grba@dh.uns.ac.rs

[1] Faculty of Technology, University of Novi Sad, Novi Sad, Serbia

[2] Faculty of Science, Department of Chemistry, Biochemistry and Environmental Protection, University of Novi Sad, Novi Sad, Serbia

[3] Faculty of Technology, University of Niš, Leskovac, Serbia